Int J Adv Manuf Technol (2017) 91:3051–3060
DOI 10.1007/s00170-017-0010-1

ORIGINAL ARTICLE

Influence of axial magnetic field on shape and microstructure of stainless steel laser welding joint

Chunming Wang[1] · **Hongwei Chen**[1] · **Zeyang Zhao**[1] · **Longchao Cao**[2] · **Ping Jiang**[2] · **Gaoyang Mi**[1]

Received: 9 August 2016 / Accepted: 4 January 2017 / Published online: 14 January 2017
© Springer-Verlag London 2017

Abstract The morphology and microstructure of the weld joint have significant influence on mechanical properties of welded specimens. In this paper, the mechanism on how the external magnetic field affected weld profile and microstructure was discussed by applying the longitudinal steady magnetic field to laser welding for SUS301 stainless steel. The optimal and scanning electron microscopes were used to measure the shape of the cross section and observe the microstructure after welding. The results showed that the shape of the cross section and microstructure could be significantly changed using the external magnetic field. Moreover, joint shape changed distinctly with the magnetic field intensity changing. With the increasing of magnetic flux density, the weld profile of the full penetration model changed from funnel to X type; meanwhile, the bottom weld width increased by 40%. In addition, the partial fusion zone occurred, and the weld width decreased by 20% while penetration increased by 18% when magnetic flux density turned into 380 mT. As far as microstructure of weld joint was concerned, it appeared that application of axial magnetic field led to indistinct fusion line and blocky austenite in big size rather than columnar grain in the center of the cross section. This phenomenon could be explained by numerical simulation results.

Keywords Magnetic field · Laser welding · Cross section shape · Microstructure · Velocity fields

1 Introduction

Laser beam welding is a new welding method with high-energy density, high efficiency, low heat input, and fine adaptability compared to conventional welding. Based on these advantages, it is widely used in the fields which ask for accuracy and quality like aerospace, electronics, railway, automobile, and medicine [1–6]. Hence, engineers are trying to expand the range of application, especially in the case of enhancing welding speed and improving seam quality, which is important to improve quality of welding products. According to previous research, the joint geometry is a very important factor to affect the welding bead quality [7–10]. Adding the magnetic field to optimize the velocity field of the welding pool is thought to be a powerful way to improve the welding quality by optimizing joint geometry [11, 12].

Over the past several years, a number of researchers have conducted experiments to investigate influence of the magnetic field on welding. Based on these experimental observations, it was found that magnetically supported laser beam welding could suppress humping, improve top bead quality, dampen plasma plume fluctuations, and increase process stability [13]. Using low-frequency magnetic fields, the flow conditions inside the melt pool can be altered, potentially enhancing melt pool dilution. The

Electronic supplementary material The online version of this article (doi:10.1007/s00170-017-0010-1) contains supplementary material, which is available to authorized users.

✉ Gaoyang Mi
nanhangmigaoyang@163.com

[1] State Key Laboratory of Material Processing and Die & Mould Technology of HUST, Huazhong University of Science and Technology, Wuhan, China

[2] State Key Laboratory of Digital Manufacturing Equipment and Technology, School of Mechanical Science and Engineering, Huazhong University of Science and Technology, Wuhan, China

frequency of the magnetic field was a critical parameter to determine the spatial distribution of elements [14]. With alternating the magnetic field, the spatial distribution of silicon at the transversal section was changed and the joint became more homogeneous for laser welding of aluminum with filler wire. The Lorentz forces induced by the magnetic field affected the horizontal component of the flow velocity at molten pool [15]. In GTA welding of austenitic stainless steel, it could be concluded that application of the axial magnetic field had an obvious effect on the shape and solidification structure of weld beads [12]. It was found that the penetration depth can be increased by more than 13% with the influence of electric and magnetic fields on plasma and keyhole of CO_2 laser welding [16]. Bachmann [17–21] and his research group studied the influence of magnetic fields on deep penetration laser welding of austenite stainless steel by using experimental and numerical investigation. The formation of gravity dropout was discussed in these works, and the prevented method was proposed in both parametrical and magnetic aspects.

According to the previous works mentioned above, the influence of the magnetic field on the macro profile and microstructure of laser welding is still insufficient which makes it difficult to execute a stable welding process. The mechanism of the velocity field at the welding pool is still unclear since it is very difficult to be observed by an experimental approach. In this work, a combined laser-magnetic welding process for SUS301 stainless steel was carried out to investigate the effect of the magnetic field on the macro profile, microstructure, and mechanical properties. The numerical model with the same condition of experiments was proposed to obtain temperature and velocity field which can be used to explain the formation mechanism of welding geometry. The relationship between welding geometry, microstructure, and mechanical properties was discussed based on the experimental and numerical results.

2 Experimental procedure

The experimental setup used in the study was schematically given in Fig. 1. Butt joint laser welding with high-power fiber laser (IPG YLR-4000) was performed on SUS301L stainless steel (150 × 100 × 2 mm, 150 × 100 × 3 mm). The chemical composition of the material is given in Table 1. The welding process was shielded by pure argon (flow rate 20 L/min). Permanent magnets (NdFeB) were located under steel plate horizontally which means that the magnetic field was vertical to the workpiece and paralleled to the laser beam. The magnet can generate not more than 490 mT of the magnetic

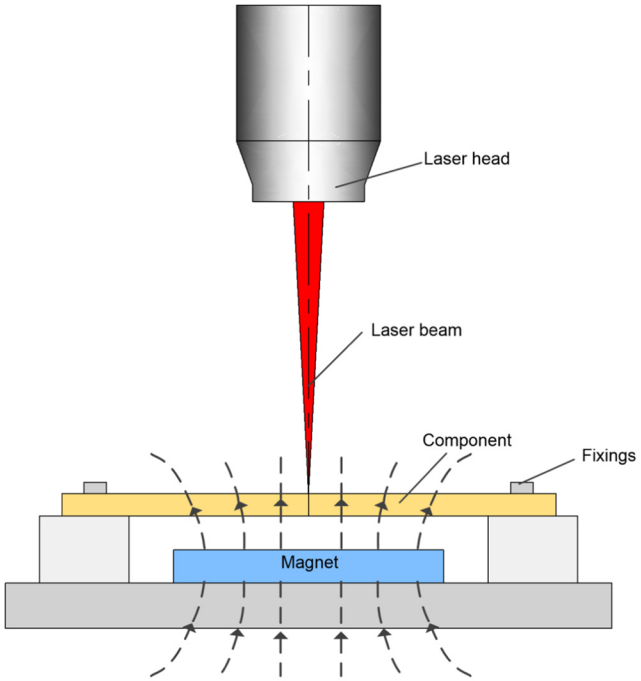

Fig. 1 Schematic representation of the experimental setup

field on the top surface, and the flux density on the top surface of the steel plate was adjusted by controlling the height of bearing shown in Fig. 1. The value of flux density on the plate was measured by a HT201 gauss meter which was used as the value of the magnetic field in the following part of the manuscript. Laser welding was carried out using a laser power of 3600 W, welding speed of 3.6 m/min, and defocusing distance of 0 mm under various magnetic field conditions (0, 95, 310, 380 mT). To measure dimensions of weld beads, transverse cross sections were made at different locations of each weld. After a standard polishing and etching process, width and penetration depth of the weld were obtained by an optic microscope. The etching reagent used to reveal the microstructure was made of one part HF, three parts HNO_3, and seven parts water. Scanning electron microscopy (SEM) was used to obtain a more microscopic observation of the microstructure. Numerical simulation of laser welding which applied axial magnetic field was carried to investigate the mechanism on how the magnetic field affects welding procedure.

Table 1 Chemical composition (wt-%) of SUS301

C	Si	Mn	P	S	Cr	Ni	N	Fe
≤0.03	≤1.0	≤2.0	≤0.045	≤0.03	18~20	8~10.5	≤0.02	Margin

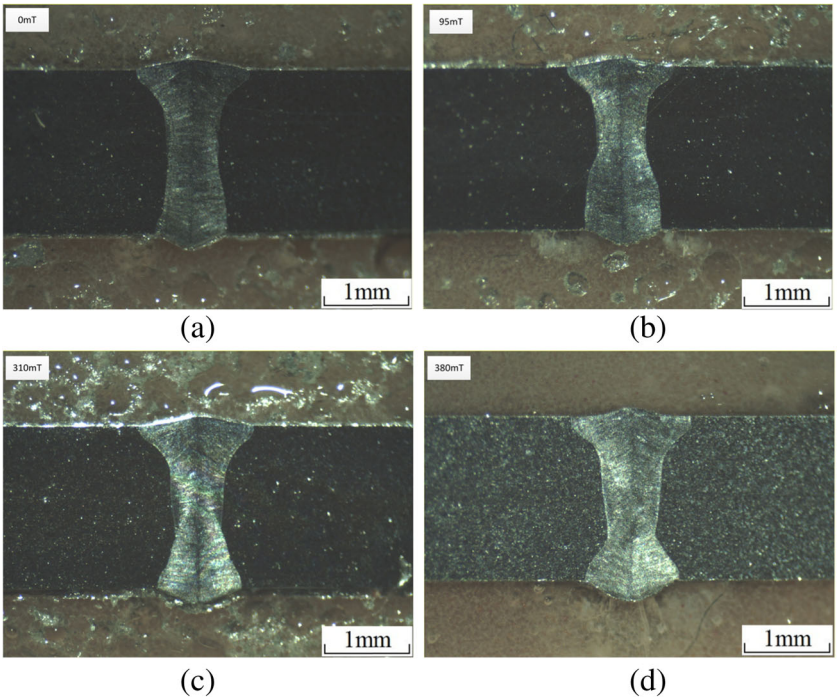

Fig. 2 The shapes of the cross section of 2-mm 301 stainless steel plates under different magnetic field

3 Results and discussion

3.1 The influence of different directions and densities of magnetic field on weld joint morphology

In theory, the shape of the cross section was only affected by heat input, which means that the joint morphology would not change with the same heat input. For laser welding, the weld width was very critical because the porosity number was directly related to weld width. A smaller weld width means a smaller welding pool would be more difficult for porosity to escape. If the weld width increased, the porosity number would decrease. According to previous research [8], increasing heat input was the only way to obtain a wider weld. However, increasing heat input was harmful for the mechanical properties, for example, increasing microstructure gradient. The shape of the cross section in laser welding also would be affected by the magnetic field [20]. It was a powerful method which could increase weld width without disadvantages caused by overheating. However, Malinowski [22] found that a 20-mT magnetic field in arc welding had a significant influence on shape and microstructure of hybrid laser-arc weld joint. When an alternating magnetic field was applied, a symmetric weld bead of regular and predictable shape was produced.

The different shapes of the cross section under 0-380mT magnetic fields are shown in Fig. 2 for a full penetrated laser welding of 2 mm stainless steel. The profile of the cross section changed from funnel to X type

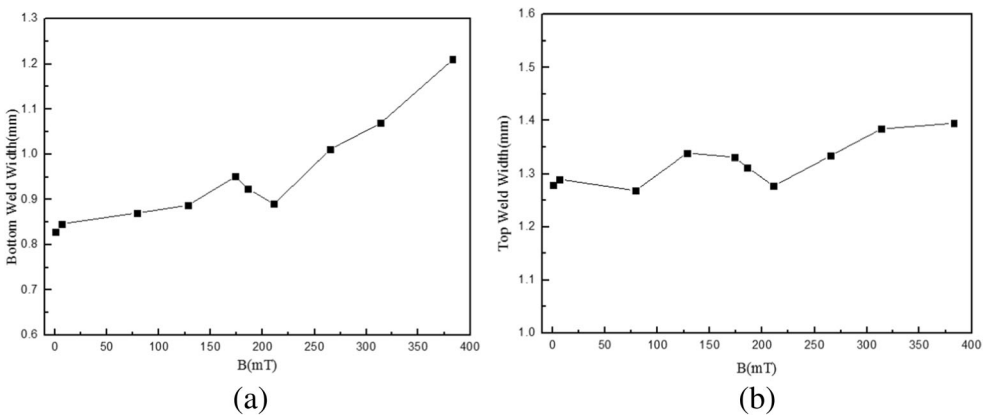

Fig. 3 Different values of top and bottom width with different magnetic densities

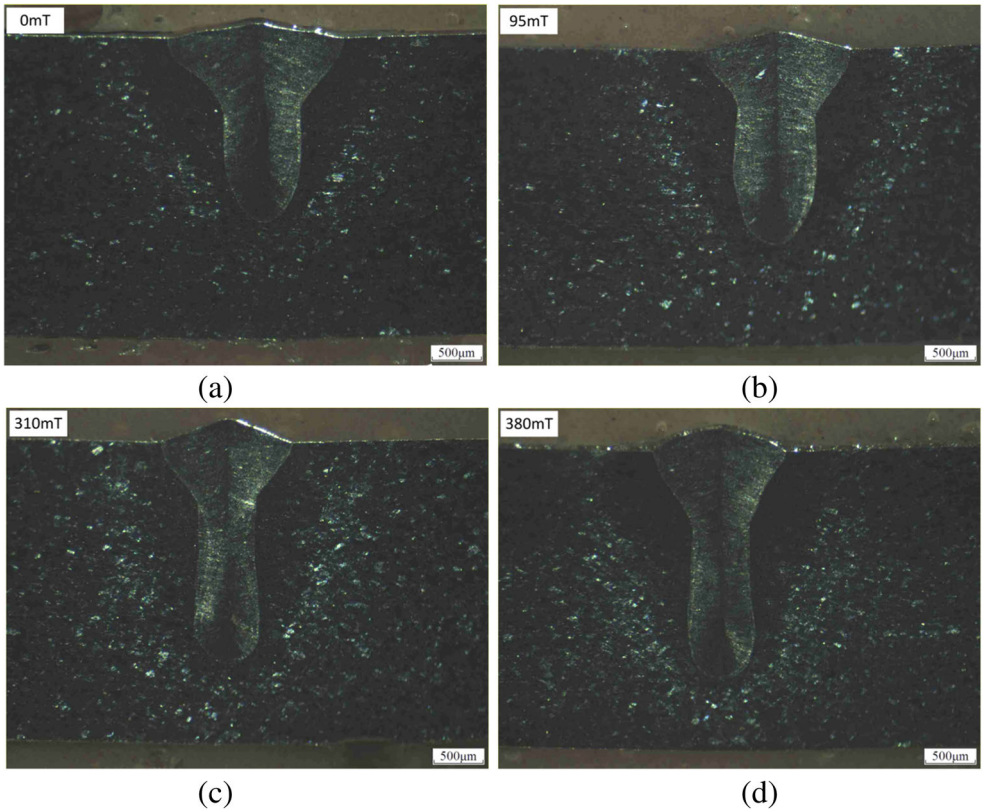

Fig. 4 The shapes of the cross section of 3-mm 301 stainless steel plates under different magnetic fields

when the magnetic density increased from 0 to 383 mT. The shape of the joint under 95 mT magnetic field had no significant difference with joint shape without the magnetic field. And yet, the top and bottom weld widths were far bigger than the middle width when applying a 380-mT magnetic field. The top and bottom widths were plotted as a function of different magnetic field strengths shown in Fig. 3. It can be concluded that seam appearance had no difference when applying a magnetic field less than 95 mT. What is more, the shape and microstructure of the weld joint stayed similar no matter how the density changed. When the magnetic density increased to 380 mT, the bottom width increased from 0.83 to 1.19 mm, which was bigger than no magnetic condition by 40%. However, the top width increased only by 10% under a 380-mT magnetic field. On the whole, with the magnetic density increasing, the values of top and bottom width were on the rise.

Likewise, it was found that the magnetic field had a significant influence on partial penetration laser welding. The cross section of 3 mm stainless steel under different magnetic fields was illustrated in Fig. 4. The value of weld width and penetration under different magnetic fields is illustrated in Fig. 5. It could be seen that the

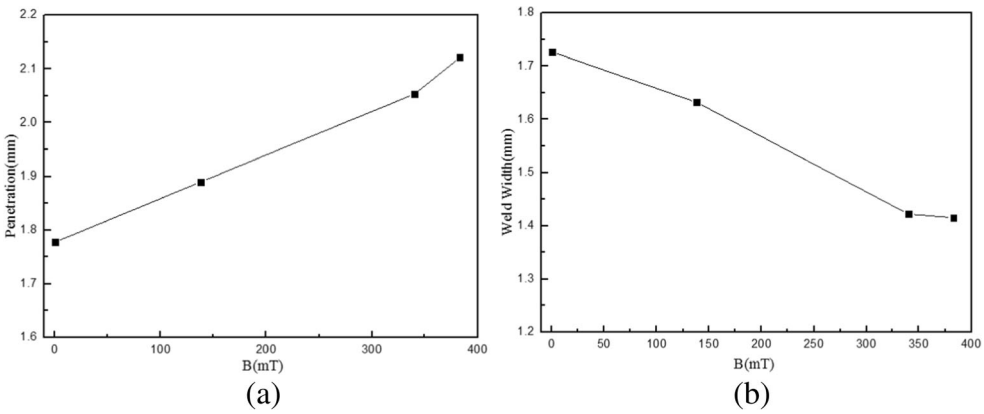

Fig. 5 Different values of width and penetration under different magnetic densities

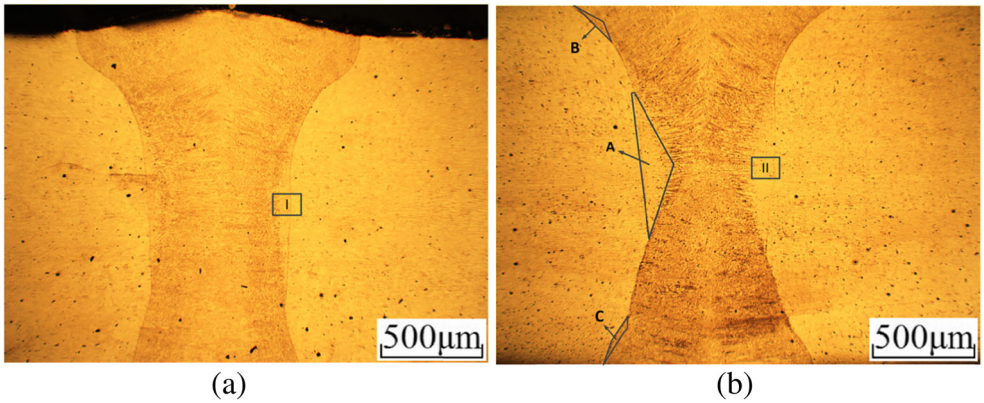

Fig. 6 Macrostructure of full penetrated 301 stainless steel weld joints. a 0 mT. b 310 mT

penetration almost increased linearly with the magnetic density increasing, while the width decreased at the same time. The shape varied from wide and shallow shape to narrow and deep shape when the magnetic density changed from 0 to 380 mT. In Fig. 5, it can be concluded that the weld width increased by 20% while penetration decreased by 18% when magnetic flux density turned into 380 mT. In conclusion, a magnetic field more than 100 mT would make a big difference on the profile of the cross section in laser welding.

3.2 Microstructure

Macro profiles of 2 mm stainless steel weld joint are shown in Fig. 6. It was observed that the fusion line was clear with no magnetic field, while the fusion line near the middle of the cross section was distinct when applying a 310-mT magnetic field. Two symmetrical triangle zones were more similar to the base metal replacing welding metal at location "A" in Fig. 6b. However, the fusion line at locations "B" (near top surface) and "C" (near bottom surface) were quiet clear. It was obvious that the shape of the fusion line was directly related to the microstructure. Aiming to study more about these zones, an optical micrograph showing the microstructures of zone I and zone II are presented in Fig. 7. Weld bead was composed of δ-ferrite and cellular dendrite, while δ-ferrite was rare in base metal. The microstructure of the base metal and weld bead was quiet different which made the fusion line very clear. However, only block austenite existed near the base metal which resulted in a fuzzy fusion line when adding a 310-mT magnetic field.

Further analysis about the partly molten zone (PMZ) was conducted by using SEM analysis. The fusion line was distinct near the black dotted line without the magnetic field. Limited δ-ferrite (light etched) distributed along the fusion line while the amount of ferrite became larger when getting closer to the centerline of the weld which was mainly composed of columnar dendrites. This phenomenon was attributed to different supercooling degrees near the base metal or near the weld centerline. The larger supercooling near the weld centerline made more δ-ferrites precipitate at the grain boundary. When combining 310 mT magnetic field with laser welding, the thermal current from liquid metal to base metal would generate Lorenz force which would stir molten pool near the base metal. The stirred molten pool would break cellular dendrites and format more blocky austenites. With a reducing temperature gradient at the welding centerline, the thermal current was too small to stir molten pool which resulted in the microstructure

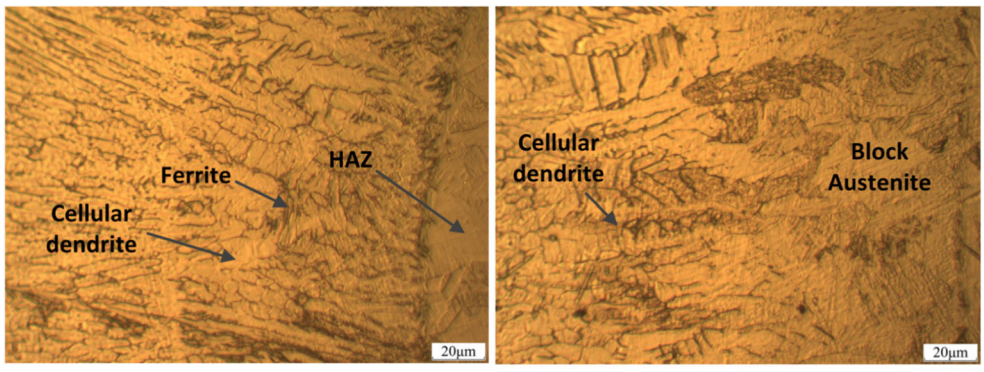

Fig. 7 Microstruture of welding metal of 301 stainless steel weld joints. **a** Zone I in Fig. 6a. b ZoneII in Fig. 6b

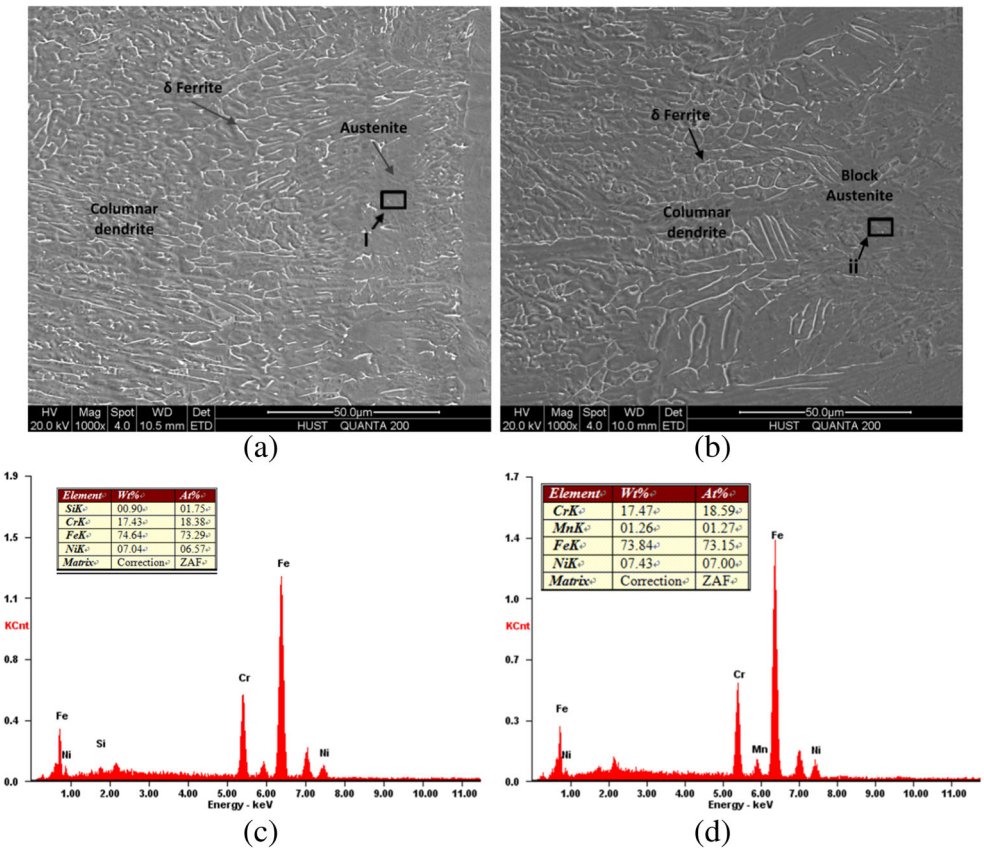

Fig. 8 SEM microstructure and spectrum analysis of middle welding metal of full penetrated 2 mm weld bead. **a** Microstructure under 0 mT. **b** Microstructure under 310 mT. **c** EDS analysis of zone I. **d** EDS analysis of zone II

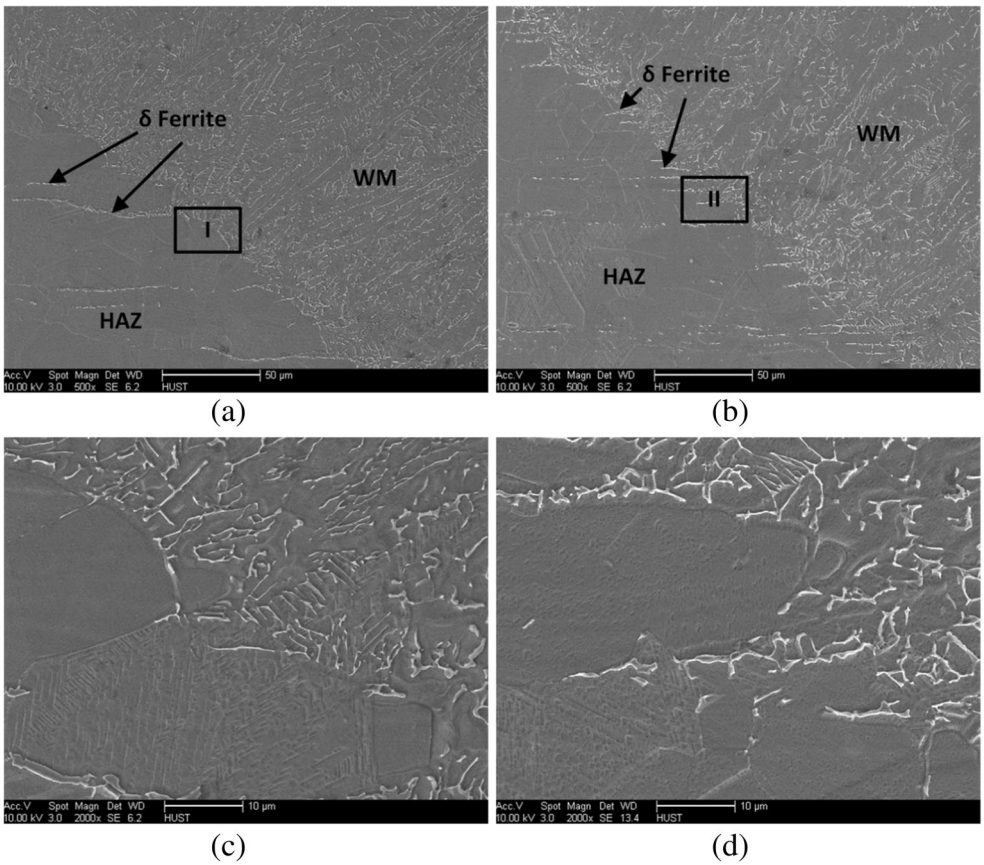

Fig. 9 SEM microstructure of full penetrated 2 mm 301 stainless steel weld joints. **a** 0 mT. **b** 310 mT. **c** Microstructure of zone I. **d** Microstructure of zone II

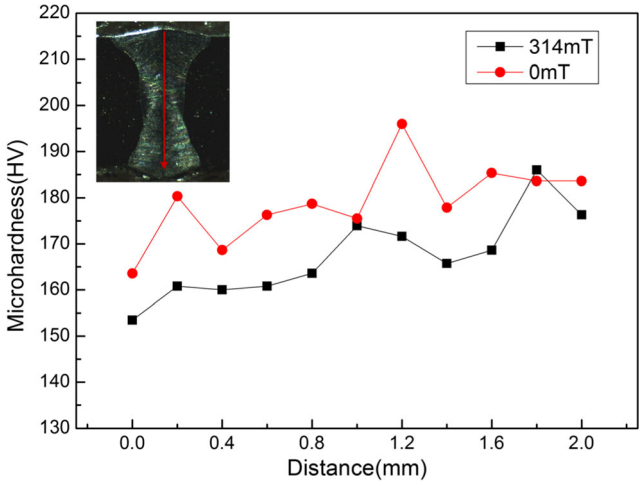

Fig. 10 Microhardness near axis of welds

mainly consisting of cellular dendrite. EDS analysis of zone I and zone II are shown in Fig. 8a, b. It was found that the chemical composition at the weld bead had no difference when the magnetic field was applied. It can be concluded that the stirred molten pool caused by thermal current showed no influence on element distribution. The changed microstructure was only attributed to the different flow velocity of the molten pool.

To study more about the influence of the magnetic field on microstructure, SEM analysis of upper weld metal is presented in Fig. 9. It could be seen that lots of vermicular δ-ferrite existed in HAZ; this could be attributed to element segregation along the rolling direction. The segregated element reduced the austenization temperature at typical location so that part of the base metal austenized and transformed to ferrite after cooling. Without the magnetic field, the amount of δ-ferrite was minor because the heat that transferred from the molten pool was very limited. However, the molten pool flowed more violently due to thermal current effect under the magnetic field. As a consequence, the base metal received more heat that transferred from the molten pool which increased both the length and amount of vermicular δ-ferrite along the rolling direction as shown in Fig. 9b.

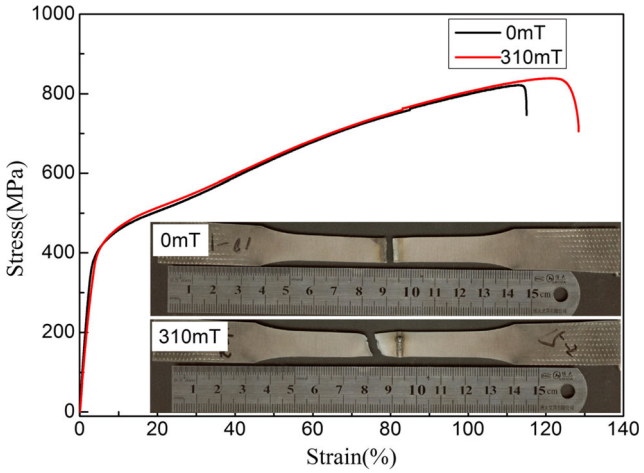

Fig. 11 Tensile property of 2 mm stainless steel welds, *upper*: 0mT, *lower*: 310mT

3.3 Mechanical properties

The microhardness of the Z-direction of joints under different magnetic conditions were measured. According to Fig. 10, the microhardness at the bottom part was bigger than that of the upper part. The microhardness under 310 mT magnetic field was totally smaller than the 0-mT magnetic field. The large phase fraction of blocky austenite was thought to be the reason for the hardness reduction. However, the difference between two magnetic fields was not more than 20 HV, which is not a large value.

The transverse tensile properties of weldment using different magnetic field conditions are shown in Fig. 11. In each condition, three specimens were tested and the average tensile was obtained to ensure repeatability. The fracture region of all weldments is cited in Table 2. There was only little difference between the strength of weld joints with or without the magnetic field. However, it can be seen that the elongation of tensile specimen under 310 mT magnetic field was obviously larger than the specimen without considering magnetic effect because of the different fracture location. The welding joint without magnetic effect, which fractured at the weld zone, exhibited much less plastic with base metal. Although the tensile strength had no big difference under different conditions, the extensibility of the weld applied magnetic field was better.

Figure 12 shows the fracture profile with 310 mT magnetic field. Pure-shear fracture mode could be obviously observed in Fig. 12a, which was resulted from the dislocation slip. The typical dimple fracture microstructure illustrated that a completely ductile fracture occurred during tensile tests. This also proved that the weld joint under 310 mT magnetic field possessed good ductility.

4 Discussion

4.1 Welding pool dynamic

Kern [13] found that the current in the weld pool was only some amperes because of the Seebeck effect. In laser welding, the electric field may exist in the molten pool, and the movement of liquid metal in the magnetic field would generate electric current. So ohm's law can be extended to be

$$ {}^{j}/_{\sigma} = e + v \times B + S\nabla T + {}^{1}/_{e}\nabla\mu \quad (1) $$

Table 2 The fracture region of weldments

B	0 mT			310 mT		
Number	1	2	3	1	2	3
Region	Weld zone	Base metal	Weld zone	Base metal	Base metal	Base metal

In formula 1, j was the current density, σ was the conductivity under isothermal condition, e was the basic electric charge, v was the speed of conductor movement which was equaled to fluid flow velocity in the molten pool, B was the magnetic induction, S was the absolute thermoelectric power, and μ was the chemical potential of liquid metal. The current caused by electric field can be ignored since there was no original field. Besides, the current caused by nonuniformity of the chemical composition did not need to be taken into consideration because composition can be regarded uniform in stainless steel. As a result, the current in laser welding molten pool can be decided only by thermoelectric current (Seeback effect) and induced current caused by the movement of conductive liquid metal in the magnetic field. So here was the discussion about Lorentz force generated by these two currents.

Compared to common welding pool, the laser welding pool under magnetic field was larger with a more intense flow. To explain this phenomenon, an assumption needs to be introduced. The assumption is that the liquid in the molten pool is approximated to the sum of charged particles so that the Lorentz equation can be applied to each particle. Since thermal current paralleled to temperature gradient (from welding pool to base metal), the induced Lorentz force was along the circumferential direction of the weld pool. The plan view of the welding pool with and without magnetic effects is shown in Fig. 13. According to Fig. 13a, most of liquid moved parallel to the temperature gradient without any circumferential component. If a magnetic field was combined, the circumferential component of velocity appeared due to the induced Lorentz force. The amount of velocity significantly increased coupling radial and circumferential components so that the movement of the molten pool became very violent. The larger size and more violent flow at the weld pool can be represented by a high-speed camera video shown in Vid. 1.

4.2 The partial fusion zone

Area "A" in Fig. 6a was named as half fusion zone because the microstructure of this part consisted of part weld and part base metal. In addition, the fusion line was blurred with no columnar grain neighboring it. Very fine equiaxed grains were found at the half fusion zone which made this area a nonsignificant crystalline orientation. The reason for this phenomenon was that columnar grains were crashed by a more intense molten pool flow caused by magnetic fields. Besides, fragments of columnar grains would stay at the welding pool in the form of impurity which was helpful for heterogeneous nucleation. Thus, a more intense flow field at the welding pool promoted the forming of equiaxed grains in one aspect and suppressed the forming of columnar grain in other aspects. However, the microstructure near the top and bottom surfaces remained to columnar grain which was quite different from the half fusion zone. The fusion line near the top and bottom surfaces was very clear. The columnar grain grew from the fusion line to the weld centerline with a single growing orientation.

The difference of the microstructure between areas "A," "B," and "C" was attributed to different supercooling degrees

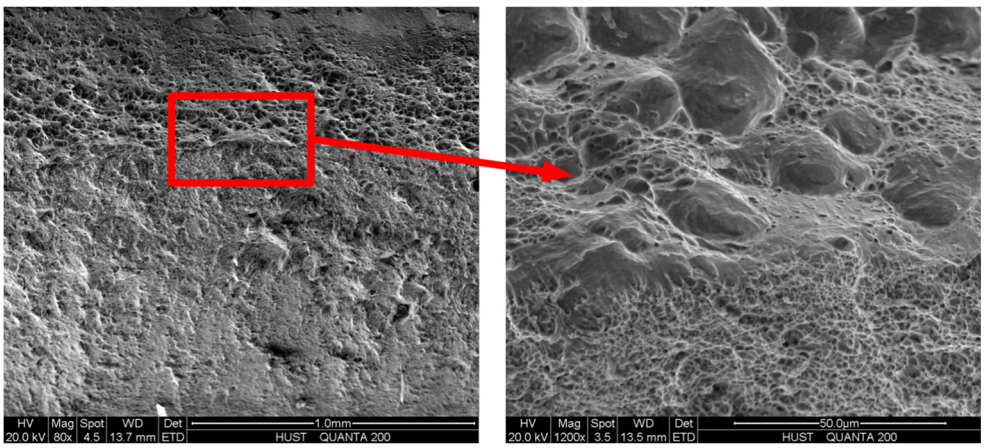

Fig. 12 SEM fracture morphology of joint under 310 mT

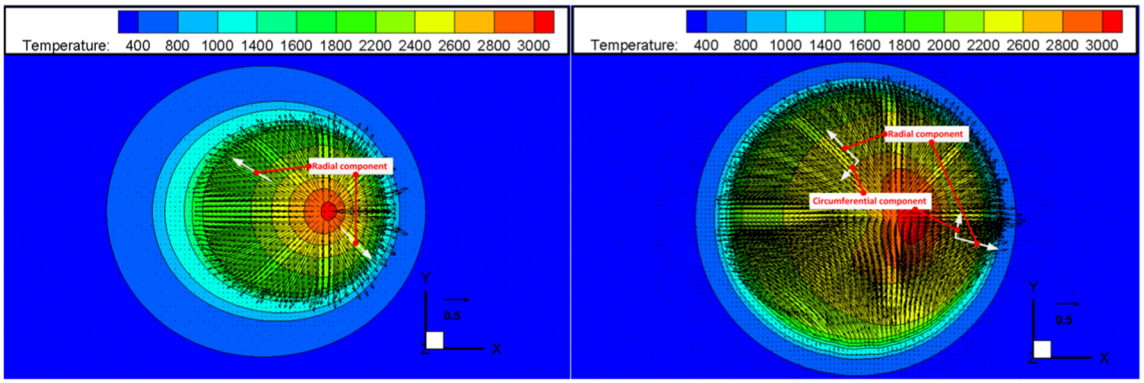

Fig. 13 Temperature field and flow field of quasi steady state. **a** Top view of laser welding molten pool without magnetic field. **b** Top view of laser welding molten with magnetic field

at different locations of the weld pool. The heat conductivity at location A was worse than that at locations B and C because no thermal convection occurred at the middle part of the weld component which made solid phase base metal at location A (at middle part of plate) remain a relatively higher temperature than locations B and C. The temperature of the molten pool boundary equaled to the melting point so that the supercooling degree at location A was smaller than those of B and C. According to welding metallurgical theory, a larger supercooling degree was helpful for generating columnar grain and the explicit growth orientation of columnar grain which was perpendicular to fusion leading to a local line anisotropy. It can be concluded that the half fusion zone occurred under the intense velocity fields caused by the magnetic field accompanied by a small supercooling degree at the middle part of the component.

5 Conclusions

1. The influence became obvious with magnetic density increasing. As the magnetic field changes from 0 to 310 mT, the weld joint varied from funnel type to X type with the bottom width increasing by 40% in full penetration laser welding 2 mm stainless steel. In addition, the shape changed from wide and shallow type to narrow and deep type with weld width decreasing by 20% while penetration increased by 18% in partial penetration laser welding. A magnetic field less than 100 mT had no significant impact on shape of the cross section in laser welding 301 stainless steel.
2. When applying an axial magnetic field bigger than 100 mT, the fusion lines in the middle of the weld joints turned into indistinct, the triangular area near the fusion line in the middle of the cross section could not be etched clearly, and the microstructure of this blur area was blocky austenite which was different with the columnar microstructure at the top and bottom surfaces.
3. A better plastic joint was obtained if the magnetic field was combined into laser welding. According to numerical simulation, the molten pool was larger and the liquid metal flow more violent considering the magnetic effect.

Acknowledgements This work was supported by the National Natural Science Foundation of China (Grant No. 51375191) and the National Natural Science Foundation of China (Grant No. 51323009). We would like to express our deep gratitude to the Analysis and Test Center of HUST (Huazhong University of Science and Technology), for their friendly cooperation.

Reference

1. Kim J, Kim S (2016) Kim Ket al. Effect of beam size in laser welding of ultra-thin stainless steel foils[J]. J Mater Process Technol 233:125–134
2. Bunaziv I, Akselsen OM, Salminen A et al (2016) Fiber laser-MIG hybrid welding of 5 mm 5083 aluminum alloy[J]. J Mater Process Technol 233:107–114
3. Casalino G, Mortello M (2015) Modeling and experimental analysis of fiber laser offset welding of Al-Ti butt joints[J]. Int J Adv Manuf Technol 83(1–4):89–98
4. Chen S, Zhai Z, Huang J et al (2015) Interface microstructure and fracture behavior of single/dual-beam laser welded steel-Al dissimilar joint produced with copper interlayer[J]. Int J Adv Manuf Technol 82(1–4):631–643
5. Correard GCC, Miranda GP, Lima MSF (2015) Development of laser beam welding of advanced high-strength steels[J]. Int J Adv Manuf Technol 83(9–12):1967–1977
6. Zhang ZH, Dong SY, Wang YJ et al (2015) Study on microstructures and mechanical properties of super narrow gap joints of thick and high strength aluminum alloy plates welded by fiber laser[J]. Int J Adv Manuf Technol 82(1–4):99–109
7. Chang B, Allen C, Blackburn J et al (2014) Fluid flow characteristics and porosity behavior in full penetration laser welding of a titanium alloy[J]. Metall Mater Trans B 46(2):906–918
8. Lu F, Li X, Li Z et al (2015) Formation and influence mechanism of keyhole-induced porosity in deep-penetration laser welding based on 3D transient modeling[J]. Int J Heat Mass Transf 90:1143–1152

9. Pang S, Chen X, Shao X et al (2016) Dynamics of vapor plume in transient keyhole during laser welding of stainless steel: local evaporation, plume swing and gas entrapment into porosity[J]. Opt Lasers Eng 82:28–40
10. Wu SC, Yu C, Zhang WH et al (2015) Porosity induced fatigue damage of laser welded 7075-T6 joints investigated via synchrotron X-ray microtomography[J]. Sci Technol Weld Join 20(1):11–19
11. Tse HC, Man HC, Yue TM (1999) Effect of electric and magnetic fields on plasma control during CO2 laser welding[J]. Opt Lasers Eng 32:55–63
12. Tse HC, Man HC, Yue TM (1999) Effect of magnetic field on plasma control during CO2 laser welding[J]. Optics & Laser Technology 31:363–368
13. Kern M, Berger P, Hugel H (2000) Magneto-fluid dynamic control of seam quality in CO2 laser beam welding[J]. Weld J 80:72–78
14. Gatzen M (2012) Influence of low-frequency magnetic fields during laser beam welding of aluminium with filler wire[J]. Phys Procedia 39:59–66
15. Gatzen M, Tang Z, Vollertsen F et al (2011) X-ray investigation of melt flow behavior under magnetic stirring regime in laser beam welding of aluminum[J]. Journal of Laser Applications 23(3): 032002
16. Lange A, Cramer A, Beyer E (2009) Thermoelectric currents in laser induced melts pools[J]. Journal of Laser Applications 21(2):82
17. Bachmann M, Avilov V, Gumenyuk A et al (2013) About the influence of a steady magnetic field on weld pool dynamics in partial penetration high power laser beam welding of thick aluminium parts[J]. Int J Heat Mass Transf 60:309–321
18. Bachmann M, Avilov V, Gumenyuk A et al (2014) Experimental and numerical investigation of an electromagnetic weld pool support system for high power laser beam welding of austenitic stainless steel[J]. J Mater Process Technol 214(3):578–591
19. Bachmann M, Kunze R, Avilov V et al (2016) Finite element modeling of an alternating current electromagnetic weld pool support in full penetration laser beam welding of thick duplex stainless steel plates[J]. Journal of Laser Applications. 28(2): 022404
20. Bachmann M, Avilov V, Gumenyuk A et al (2016) Numerical assessment and experimental verification of the influence of the Hartmann effect in laser beam welding processes by steady magnetic fields[J]. Int J Therm Sci 101:24–34
21. Bachmann M, Avilov V, Gumenyuk A et al (2012) Numerical simulation of full-penetration laser beam welding of thick aluminium plates with inductive support[J]. J Phys D Appl Phys 45(3):035201
22. Malinowski M, Ouden G, Vick W (1990) Effect of electromagnetic stirring on GTA welds in austenitic stainless steel[J]. Weld J 69(2): 59–66